AIP | Applied Physics Letters

Nb-doped single crystalline MoS2 field effect transistor

Saptarshi Das, Marcellinus Demarteau, and Andreas Roelofs

Citation: Applied Physics Letters **106**, 173506 (2015); doi: 10.1063/1.4919565
View online: http://dx.doi.org/10.1063/1.4919565
View Table of Contents: http://scitation.aip.org/content/aip/journal/apl/106/17?ver=pdfcov
Published by the AIP Publishing

Nb-doped single crystalline MoS_2 field effect transistor

Saptarshi Das,[1,2,a)] Marcellinus Demarteau,[2] and Andreas Roelofs[1]
[1]*Center for Nanoscale Material, Argonne National Laboratory, Argonne, Illinois 60439, USA*
[2]*Division of High Energy Physics, Argonne National Laboratory, Argonne, Illinois 60439, USA*

(Received 18 February 2015; accepted 20 April 2015; published online 29 April 2015)

We report on the demonstration of a p-type, single crystalline, few layer MoS_2 field effect transistor (FET) using Niobium (Nb) as the dopant. The doping concentration was extracted and determined to be $\sim 3 \times 10^{19}/cm^3$. We also report on bilayer Nb-doped MoS_2 FETs with ambipolar conduction. We found that the current ON-OFF ratio of the Nb-doped MoS_2 FETs changes significantly as a function of the flake thickness. We attribute this experimental observation to bulk-type electrostatic effect in ultra-thin MoS_2 crystals. We provide detailed analytical modeling in support of our claims. Finally, we show that in the presence of heavy doping, even ultra-thin 2D-semiconductors cannot be fully depleted and may behave as a 3D material when used in transistor geometry. Our findings provide important insights into the doping constraints of 2D materials, in general. © *2015 AIP Publishing LLC*. [http://dx.doi.org/10.1063/1.4919565]

Over the last few years, interest in two dimensional semiconducting materials beyond graphene has grown exponentially across all scientific and engineering disciplines. Transition metal dichalcogenides (TMDs), with the general formula of MX_2 (where M = Mo and W and X = S, Se, and Te), are particularly promising in the context of solid state devices due to their unique electrical transport properties.[1–10] Unlike graphene, these semiconducting TMDs possess a finite bandgap in the range of 0.7–1.2 eV in a few layers, which is most desirable for logic transistor applications. In addition, the TMDs naturally allow excellent electrostatic gate control due to their atomistically thin body dimension.

However, there are many challenges that remain to be solved before the TMDs can be commercially implemented. One of these challenges is the accessibility of both the electrons (n-type carriers) in the conduction band and holes (p-type carriers) in the valence band so that complementary device operations can be executed. Contact engineering, whereby the position of the metal Fermi level is adjusted relative to the band structure of the semiconductor, has been used in the first generation of TMD field effect transistors (FETs) to partially achieve this objective.[11–14] For example, conventional metal contacts like Sc, Ti, Ni, and Au were found to facilitate electron transport in MoS_2, while high work function MoO_x contacts allowed efficient hole injection in MoS_2.[2,11,12] However, such metal-semiconductor contacts are invariably associated with Schottky barriers that limit the device performance. Replacing the metal electrode with graphene seems to provide a unique way to enhance ambipolar conduction (presence of both electron and hole transport) in the TMDs and also reduce the contact resistance considerably.[15–18]

In this article, we report substitutional doping of MoS_2 with Niobium (Nb) as a promising way to enhance hole transport in MoS_2. Nb-doped MoS_2 crystals obtained from www.hqgraphene.com were mechanically exfoliated on 100 nm thick SiO_2 layers with highly doped Si as the substrates. Conventional scotch tape technique was used to peel off the Nb-doped MoS_2 layers from the crystals. Optical lithography (laser writer) was used to pattern the Source/Drain contacts, and electron beam evaporation was used to deposit 80 nm thick Ni as the contact metal. Figure 1(a) shows the AFM image of a prototype Nb-doped MoS_2 transistor gated from the back and Figure 1(b) shows the device structure schematically.

Figure 2(a) shows the room temperature transfer characteristics of a 20 nm thick Nb-doped MoS_2 FET for different source to drain biases (V_{DS}) in logarithmic scale. Figure 2(b) shows the output characteristics of the same device for different over-drive voltages ($V_{DRIVE} = V_{BG} - V_{TH}$, where V_{BG} is the back gate voltage and V_{TH} is the threshold voltage). Figure 2(c) shows the transfer characteristics of an intrinsic (or rather, not intentionally doped) MoS_2 FET with similar flake thickness in logarithmic scale. The intrinsic MoS_2 FET shows n-type device characteristics in accordance with our earlier findings,[2,3] while the Nb-MoS_2 FET shows p-type device characteristics. Moreover, the Nb-doped MoS_2 FET shows poor ON/OFF current ratio and an almost complete loss of gate control beyond a certain V_{BG}.

In order to explain the characteristics the Nb-doped MoS_2 FET, we invoke a simple model which is described in Figure 3. Figure 3(a) shows the energy band diagram of a metal-oxide-semiconductor (MOS) interface for a p-type semiconductor under depletion condition ($V_{DRIVE} > 0$). E_C and E_V are, respectively, the conduction and valence band edges of the semiconductor. E_{FS} and E_{FM} are the Fermi level of the semiconductor and the metal, respectively. $0 < X < W_{DM}$ is the surface depletion layer and t_{BODY} is the thickness of the semiconductor channel. The maximum width of the depletion layer (W_{DM}) is given by the following equations:

$$W_{DM} = \sqrt{\frac{4\varepsilon_s kT \ln(N_A/n_i)}{q^2 N_A}}, \tag{1a}$$

$$n_i = \sqrt{N_C N_V} \exp\left(-\frac{E_G}{2kT}\right), \tag{1b}$$

a)Author to whom correspondence should be addressed. Electronic addresses: das.sapt@gmail.com and das@anl.gov

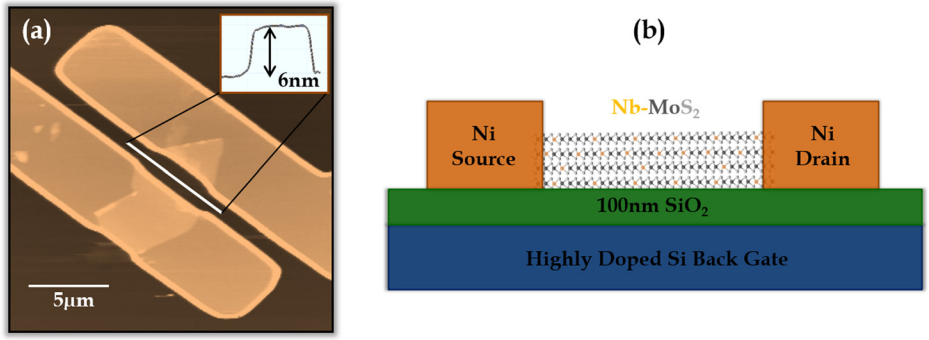

FIG. 1. (a) AFM image of a 6 nm thick Nb-doped MoS_2 flake (inset shows the height profile) and (b) schematic device structure of a back gated FET on 100 nm SiO_2 substrate with Ni.

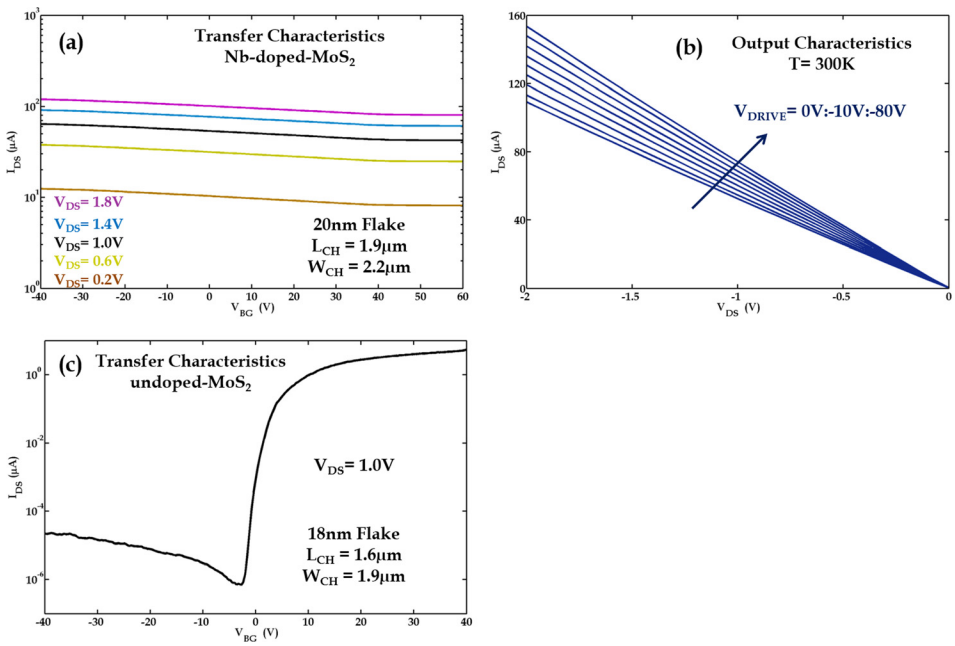

FIG. 2. (a) Transfer characteristics of Nb-doped MoS_2 back gated FET with flake thickness of ~20 nm for different V_{DS} at room temperature. (b) Output characteristics of the same device for different over-drive voltages. (c) Transfer characteristics of an undoped MoS_2 FET with similar flake thickness (~18 nm) for $V_{DS} = 1.0$ V.

$$N_C = 2\sqrt{2\pi m_n kT/h^2}, \quad N_V = 2\sqrt{2\pi m_p kT/h^2}, \qquad (1c)$$

where ε_S is the dielectric constant of the semiconductor (along the x-direction), N_A and n_i are, respectively, the extrinsic and intrinsic doping concentrations, q is the electronic charge, k is the Boltzmann constant, T is the temperature, E_G is the bandgap of the semiconductor, and m_n and m_p are the effective masses for the electron and holes, respectively.[19]

In a MOS geometry, the gate voltage can control the band movement in the channel for $x < W_{DM}$. Therefore, if

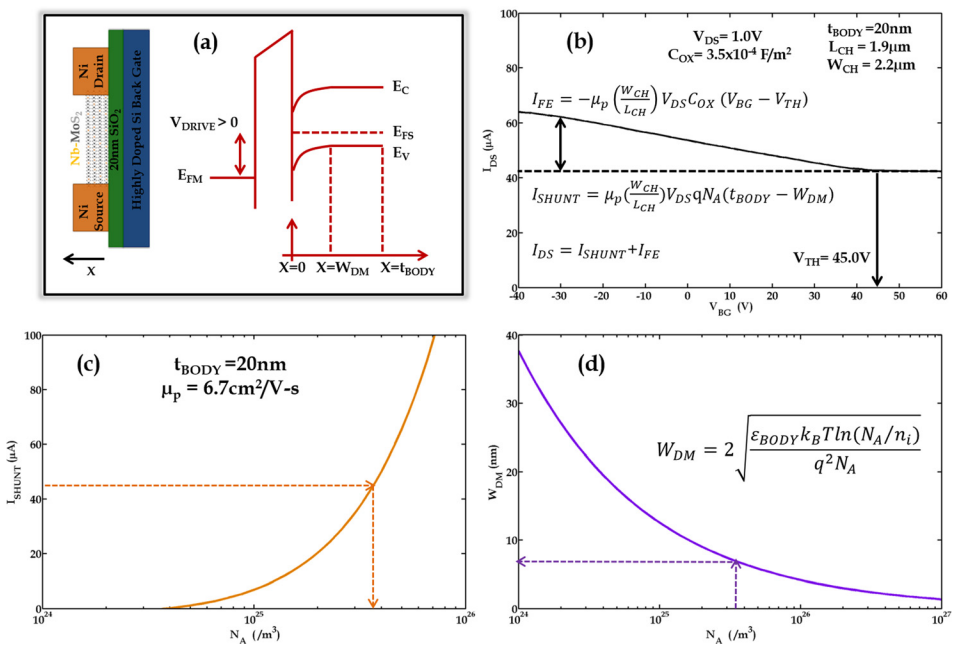

FIG. 3. (a) Energy band diagram of a metal-oxide-semiconductor interface (p^{++}Si—20 nm SiO_2–Nb doped MoS_2) under depletion condition. (b) Experimental transfer characteristics of 20 nm thick Nb-doped MoS_2 flake showing the different components (I_{FE} and I_{SHUNT}) of source to drain current (I_{DS}) and their dependence on V_{BG} for $V_{DS} = 1.0$ V. (c) Simulated shunt current with field effect hole mobility of ~5 cm^2/Vs and (d) simulated maximum width of the depletion region as a function of the extrinsic doping concentration.

the thickness of the semiconducting channel is more than the maximum width of the depletion region ($t_{BODY} > W_{DM}$), the device cannot be fully depleted even under strong inversion conditions. In our Nb-doped MoS_2 FET, this is what causes a shunting path for the current and prevents the device from being completely turned OFF. A detailed analysis of this shunting current allows us to extract the doping concentration in the MoS_2 flakes. Figure 3(b) shows the different components of the source to drain current ($I_{DS} = I_{FE} + I_{SHUNT}$) in the 20 nm thick Nb-doped MoS_2 flake as a function of V_{BG} for $V_{DS} = 1.0$ V. The field effect current I_{FE} is the current associated with the depletion layer and follows the conventional gate voltage dependence given by the following equation:

$$I_{FE} = \mu_p \left(\frac{W_{CH}}{L_{CH}}\right) V_{DS} C_{OX} \left(V_{BG} - V_{TH}\right), \qquad (2)$$

where μ_p is the hole mobility, W_{CH} and L_{CH} are the channel width and channel length, respectively, and C_{OX} is the oxide capacitance. Also, $C_{OX} = \varepsilon_{OX}/d_{OX}$, where ε_{OX} is the dielectric constant and d_{OX} is the thickness of the gate oxide, $d_{OX} = 100$ nm and for SiO_2, $\varepsilon_{OX} = 3.5 \times 10^{-11}$ F/m, which gives $C_{OX} \sim 3.5 \times 10^{-4}$ F/m^2. Note that the only unknown in the above equation is μ_p, which can be extracted from the slope of the I_{FE} *versus* V_{BG} plot. The magnitude of μ_p was found to be 6.7 cm^2/V-s. The shunting current (I_{SHUNT}), on the contrary, is associated with the undepleted region of the semiconducting channel ($W_{DM} < X < t_{BODY}$) and as explained above is independent of the applied gate voltage. This portion of the semiconducting channel acts like a simple resistor and, therefore, I_{SHUNT} is given by the following equation:

$$I_{SHUNT} = \mu_p \left(\frac{W_{CH}}{L_{CH}}\right) V_{DS} q N_A (t_{BODY} - W_{DM}). \qquad (3)$$

Figures 3(c) and 3(d), respectively, show the shunting current and the maximum width of the depletion region as a function of the extrinsic doping concentration N_A calculated using Eqs. (1) and (3). In our 20 nm Nb-doped MoS_2, $I_{SHUNT} = 43\ \mu$A, which corresponds to an $N_A = 3.3 \times 10^{19}$/cm^3 for the MoS_2 crystal and hence $W_{DM} = 7.8$ nm. The Nb-doped MoS_2 crystals can be stoichiometrically represented as $Mo_{(1-x)}Nb_xS_2$, where x is the mole fraction of Nb. The quantity x can be calculated as the product of the volume of a unit cell and the dopant concentration (per unit volume). $x = \frac{\sqrt{3}}{2} a^2 c N_A$, where a = 3.12 Å and c = 12.8 Å are the in-plane and out of plane lattice constants of MoS_2, respectively.[20] We found x = 0.02 for our Nb-doped MoS_2 crystals.

Figures 4(a) and 4(b) show the transfer and output characteristics of a bi-layer Nb-doped MoS_2 flake from the same crystal. Since the flake thickness ($t_{BODY} \sim 1.5$ nm) is less than W_{DM} (~8 nm); the device can be completely turned OFF with ON/OFF current ratio being more than 10^5. In fact, the device can be inverted as well to obtain electron transport. The band diagram associated with different region of the device characteristics are shown in Figure 4(c). Please note that the intrinsic nature ($I_{DS} \sim 0$) of the device characteristics at $V_{BG} = 0$ V is related to the shift in threshold voltage due to flat band condition and does not invoke any concern regarding the p-type doping in ultra-thin MoS_2 flakes. Also note that the symmetric ambipolar nature of the bi-layer device is a clear indication of the fact that the Ni Fermi level at the source and the drain contacts is aligned with the middle of the bandgap of Nb-doped MoS_2. Using a technique described in our earlier article,[21] we found the Schottky barrier height to be 0.52 eV for both electron and holes at the Ni-MoS_2 interface and the bandgap of Nb-doped MoS_2 to be 1.04 eV.

Figure 5(a) shows the transfer characteristics of Nb-doped MoS_2 FETs with different flake thicknesses. As expected, the FETs with flake thicknesses more than W_{DM} do not show good ON/OFF current ratio. However, it is interesting to note that the OFF current shows a monotonic trend even for flakes with thicknesses less than W_{DM}. This cannot be explained using the piecewise linear model described above, which assumes that the shunting effect arises only for the part of the semiconducting channel which is thicker than W_{DM}. In reality, complete depletion of carriers happens only at the interface between the oxide and the semiconducting channel. The local

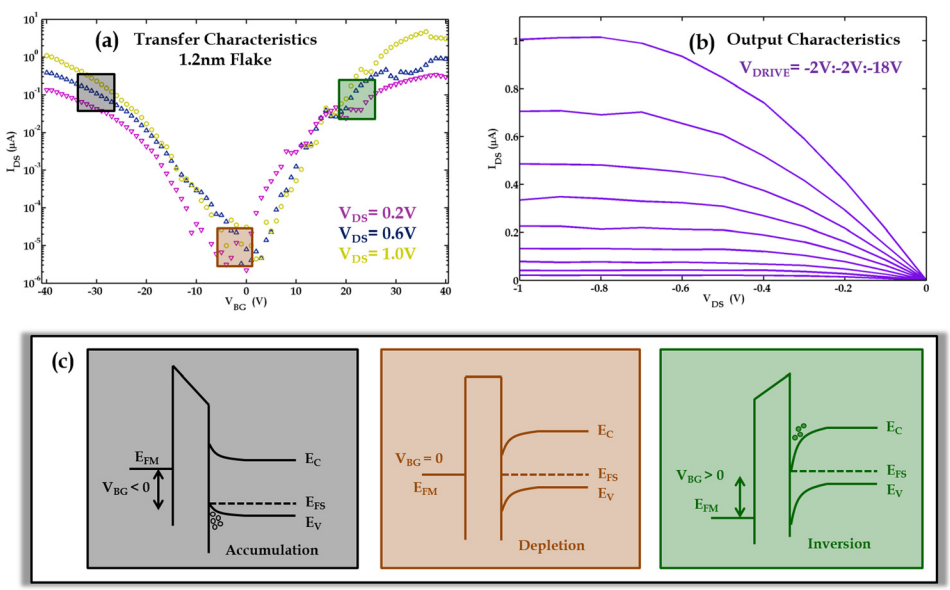

FIG. 4. (a) Transfer and (b) output characteristics of bi-layer Nb-doped MoS_2 FET at room temperature. (c) Band diagram associated with different regions (accumulation, depletion, and inversion) of the device operation.

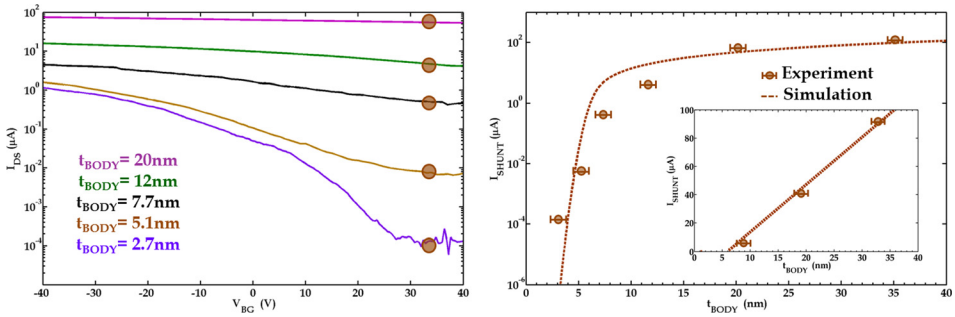

FIG. 5. (a) Transfer characteristics of Nb-doped MoS_2 FETs for different flake thicknesses at room temperature. (b) Simulation and experimental data show that the OFF current increases monotonically as a function of the flake thickness.

carrier concentration at a distance X from the surface is given as follows:

$$n(X) = n_i \exp\left[\frac{q(\psi_B - \psi(X))}{kT}\right], \quad \psi_B = \frac{kT}{q}\ln\frac{N_A}{n_i}$$
$$\psi(X) = \begin{cases} 2\psi_B\left(1 - \dfrac{X}{W_{DM}}\right)^2 & \text{for } X < W_{DM} \\ 0 & \text{for } X > W_{DM}. \end{cases} \quad (4)$$

All these carriers could potentially contribute to the shunting current. Figure 5(b) shows the I_{SHUNT} as a function of the body thickness calculated by integrating the charges described in the above equation over the thickness of the flake (t_{BODY}). We found that I_{SHUNT} changes exponentially as a function of the body thickness for $t_{BODY} < W_{DM}$. However, for $t_{BODY} > W_{DM}$, the dependence becomes linear (inset of Figure 5(b)) which was accurately captured in our discussion for Figure 3 using Eq. (3). Note that our experimental data match with this model fairly well.

Finally Figure 6 shows the simulated ON/OFF current ratio as a function of the flake thickness for different doping concentrations. Since higher doping concentrations are associated with smaller depletion width, the shunting effect becomes more dominant even for thin flakes and reduces the ON/OFF current ratio. Therefore, heavily doped ultra-thin 2D MoS_2 flakes could potentially behave similar to a bulk semiconductor when used in MOS geometry. The reader should note that the reduced ON/OFF ratio in a field effect transistor characteristics could be a result of reduced bandgap. However, in such instances, the device characteristics should become more "Ambipolar." But in our study, the shunt current dominates and obscures the regular electron branch. So the effect of bandgap change is experimentally indistinguishable.

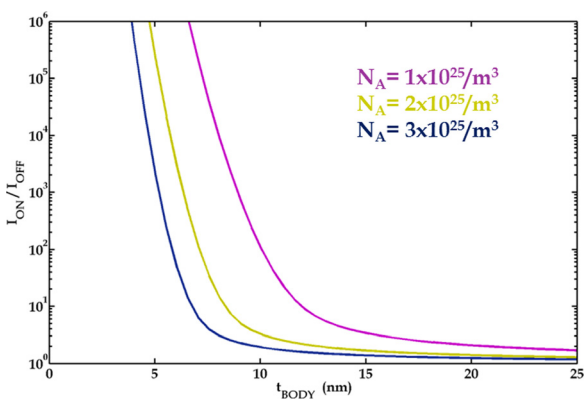

FIG. 6. Dependence of the ON/OFF current ratio on the flake thickness for different extrinsic doping concentrations.

In conclusion, we characterized single crystalline MoS_2 FETs with Nb doping, while bi-layer flakes show ambipolar conduction and thicker flakes show only p-type characteristics. The ON/OFF current ratio decreases monotonically as the flake thickness is increased due to shunting effect from the undepleted portion of the flakes. Our findings determine the doping constraints of ultra-thin 2D materials, in general.

The work of Saptarshi Das was supported by the DOE Office of High Energy Physics under DoE Contract No. DE-AC02-06CH11357. Use of the Center for Nanoscale Materials was supported by the U.S. Department of Energy, Office of Science, Office of Basic Energy Sciences, under Contract No. DE-AC02-06CH11357.

S.D. designed, conceived, and performed the experiments. S.D., M.D., and A.R. wrote the main manuscript. All authors reviewed the manuscript.

The authors declare no competing financial interests.

[1]B. Radisavljevic, A. Radenovic, J. Brivio, V. Giacometti, and A. Kis, "Single-layer MoS_2 transistors," Nat. Nanotechnol. **6**, 147–150 (2011).
[2]S. Das, H. Chen, A. V. Penumacha, and J. Appenzeller, "High performance multilayer MoS_2 transistors with scandium contacts," Nano Lett. **13**, 100–105 (2013).
[3]S. Das and J. Appenzeller, "Screening and interlayer coupling in multilayer MoS_2," Phys. Status Solidi RRL **7**, 268–273 (2013).
[4]H. Fang, S. Chuang, T. C. Chang, K. Takei, T. Takahashi, and A. Javey, "High-performance single layered WSe_2 p-FETs with chemically doped contacts," Nano Lett. **12**, 3788–3792 (2012).
[5]V. Podzorov, M. E. Garshenson, Ch. Kloc, R. Zeis, and E. Bucher, "High-mobility field-effect transistors based on transition metal dichalcogenides," Appl. Phys. Lett. **84**, 3301 (2004).
[6]N. R. Pradhan, D. Rhodes, S. Feng, Y. Xin, S. Memaran, H. B. Moon, H. Terrones, M. Terrones, and L. Balicas, "Field effect transistor based on few-layered-α-$MoTe_2$," ACS Nano **8**, 5911–5920 (2014).
[7]W. S. Hwang, M. Remskar, R. Yan, V. Protasenko, K. Tahy, S. D. Chae, P. Zhao, A. Konar, H. Xing, A. Seabaugh, and D. Jena, "Transistors with chemically synthesized layered semiconductor WS_2 exhibiting 10^5 room temperature modulation and ambipolar behavior," Appl. Phys. Lett. **101**, 013107 (2012).
[8]S. Das and J. Appenzeller, "Where does the current flow in two-dimensional layered systems?," Nano Lett. **13**, 3396–3402 (2013).
[9]S. Larentis, B. Fallahazad, and E. Tutuc, "Field effect transistors and intrinsic mobility in ultra-thin $MoSe_2$ layers," Appl. Phys. Lett. **101**, 223104 (2012).
[10]L. Liu, S. Balakumar, Y. Ouyang, and J. Guo, "Performance limits of monolayer transition metal dichalcogenide transistors," IEEE Trans. Electron Devices **58**, 3042–3047 (2011).
[11]S. Chuang, C. Battaglia, A. Azcatl, S. McDonnell, J. S. Kang, X. Yin, M. Tosun, R. Kapadia, H. Fang, R. Wallace, and A. Javey, "MoS_2 p-type transistors and diodes enabled by high work function MoO_x contacts," Nano Lett. **14**, 1337–1342 (2014).

[12]S. Das, A. Prakash, R. Salazar, and J. Appenzeller, "Toward low power electronics: Tunneling phenomena in TMDs," ACS Nano **8**, 1681–1689 (2014).
[13]S. Das and J. Appenzeller, "WSe_2 field effect transistors with enhanced ambipolar characteristics," Appl. Phys. Lett. **103**, 103501 (2013).
[14]S. Das, M. Dubey, and A. Roelofs, "High gain, low noise fully complementary logic inverter based on bilayer WSe_2 field effect transistors," Appl. Phys. Lett. **105**, 083511 (2014).
[15]J. Y. Kwak, J. Hwang, B. Calderon, H. Asalman, N. Munoz, B. Schutter, and M. Spencer, "Electrical characteristics of multilayer MoS_2 FET's with MoS_2/graphene heterojunction contacts," Nano Lett. **14**, 4511–4516 (2014).
[16]Y. T. Lee, K. Choi, H. S. Lee, S. Min, P. J. Jeon, D. K. Hwang, H. J. Choi, and S. Im, "Graphene versus Ohmic metal as source drain electrode for MoS_2 nanosheet transistor channel," Small **10**, 2356–2361 (2014).
[17]S. Das, R. Gulotty, A. Sumant, and A. Roelofs, "All two dimensional, flexible, transparent and thinnest thin film transistors," Nano Lett. **14**, 2861–2866 (2014).
[18]Y. Du, L. Yang, J. Zhang, H. Liu, K. Majumdar, P. D. Kirsch, and P. D. Ye, "MoS_2 field-effect transistors with graphene/metal heterocontacts," IEEE Electron Device Lett. **35**, 599–601 (2014).
[19]S. M. Sze, *Semiconductor Devices: Physics and Technology*, 2nd ed. (John Wiley & Sons, Singapore, 2001).
[20]E. Kadantsev and P. Hawrylak, "Electronic structure of a single MoS_2 monolayer," Solid State Commun. **152**, 909–913 (2012).
[21]S. Das, M. Demarteau, and A. Roelofs, "Ambipolar phosphorene field effect transistor," ACS Nano **8**, 11730–11738 (2014).